arXiv:1610.02817v1 [cond-mat.mes-hall] 10 Oct 2016

Spintronics via non-axisymmetric chiral skyrmions

A. O. Leonov,[1,2,3,*] J. C. Loudon,[4] and A. N. Bogdanov[1,2]

[1] *Center for Chiral Science, Hiroshima University, Higashi-Hiroshima, Hiroshima 739-8526, Japan*
[2] *IFW Dresden, Postfach 270016, D-01171 Dresden, Germany*
[3] *Zernike Institute for Advanced Materials, University of Groningen, Groningen, 9700AB, The Netherlands*
[4] *Department of Materials Science and Metallurgy, 27 Charles Babbage Road, Cambridge, CB3 0FS, United Kingdom*

(Dated: October 11, 2016)

Micromagnetic calculations demonstrate a peculiar evolution of non-axisymmetric skyrmions driven by an applied magnetic field in confined helimagnets with longitudinal modulations. We argue that these specific solitonic states can be employed in nanoelectronic devices as an effective alternative to the common axisymmetric skyrmions which occur in magnetically saturated states.

PACS numbers: 75.30.Kz, 12.39.Dc, 75.70.-i.

Two-dimensional topological solitons with an axisymmetric structure (commonly addressed as isolated *chiral skyrmions*[1]) are stabilized by Dzyaloshinskii-Moriya interactions in the *saturated* states of noncentrosymmetric magnetic materials[2]. In magnetic nanolayers, chiral skyrmions represent nanosized spots of reverse magnetization which can be created or deleted by a magnetic tip[3] and moved by electric currents and applied magnetic fields[1,3,4]. Due to their remarkable properties, magnetic skyrmions are considered promising objects for next-generation memory and logic devices[5–7], which store information in the form of skyrmions that can be manipulated at room temperature[8–10].

In practice, isolated magnetic skyrmions are induced and manipulated in laterally confined saturated helimagnets (slabs, narrow strips, nanowires, and nanodots)[1,3,7,11,12]. Importantly, magnetic saturation is never fully reached in confined nanosystems as surface modulations occur near the sample edges (so called *chiral surface twists*)[13] with a *penetration depth* estimated as 0.1 p (p is the helix period at zero field)[14]. In the case of a narrow strip, the edge states manifest themselves as remnants of the helical spiral[14–16] with a smooth deviation of the magnetization from being co-aligned with the field in the middle of the sample (Fig. 1 (a), (b)) to composing some (field- and anisotropy-dependent) angle θ_0 at the edge. To date, theoretical investigations of confined chiral skyrmions and their applications have been restricted to saturated helimagnets (Fig. 1(b))[6,17]. In that case, the skyrmion-edge interaction has a repulsive character (Eq. (21) in Ref. 14) due to the same rotational sense of the magnetization in the *axisymmetric* skyrmions and the surface modulations.

In this Letter we address a special type of *non-axisymmetric* skyrmion introduced in Ref. 18. These three-dimensional solitonic states arise in longitudinally modulated chiral ferromagnets (with the conical phase, Fig. 1 (c)) and hence are inhomogeneous along their axes. Within the micromagnetic model we calculate the structure of non-axisymmetric skyrmions and edge modulations in a confined chiral helimagnet. We show that the conical phase turns the skyrmion-edge repulsion into an attraction and consequently, there is an equilibrium distance from the edge at which the force on the skyrmions is zero. This equilibrium distance can be tuned by changing the applied magnetic field and it acts to guide the skyrmions along the edges. We demonstrate that specific properties of confined non-axisymmetric skyrmions offer new directions in spintronic applications of chiral skyrmions.

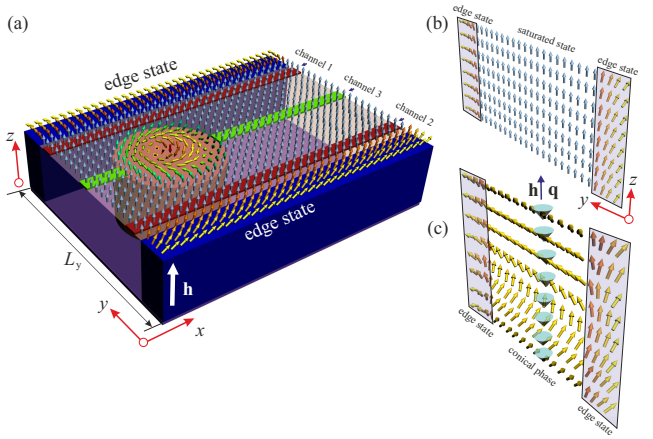

FIG. 1. (color online). (a) Schematic of the motion of an isolated skyrmion in a film infinite in the x and z directions (periodic boundary conditions with period p are used for these coordinates) and confined by parallel planes at $y = 0; L_y$. At high magnetic fields with H parallel to z ($H > H_D$), axisymmetric skyrmions exist within the magnetically saturated matrix. Repulsive edge modulations force axisymmetric skyrmions to locate along the middle line of the sample (indicated with the *green* line). For $H < H_D$ the saturated state transforms into the longitudinally modulated (*cone*) phase with the propagation vector $\mathbf{q}$ along the field, and skyrmions become non-axisymmetric and inhomogeneous along the thickness (see model (1)). In this case, under the influence of attractive interactions with the edge states, the skyrmions are situated along facets of the sample (indicated by two red strips). (b) and (c) schematically show the structure of the homogeneous and the conical phases in the yz cross section, correspondingly.

The outline of this article is as following: first, we investigate the structure of the edge states arising in the conical phase at the lateral boundaries of the system (Fig. 2). We do not include isolated skyrmions at this stage. Then, we proceed with a brief theoretical overview of isolated skyrmions within the conical phase without any influence of the edge states (Fig. 3). Based on this, we finally consider edge-skyrmion attraction in Fig. 4.

The equilibrium solutions for skyrmions and edge modulations are derived within the standard discrete model of a chiral ferromagnet where the total energy is given by:

$$w = J \sum_{<i,j>} (\mathbf{S}_i \cdot \mathbf{S}_j) - \sum_i \mathbf{H} \cdot \mathbf{S}_i - D \sum_i (\mathbf{S}_i \times \mathbf{S}_{i+\hat{x}} \cdot \hat{x} + \mathbf{S}_i \times \mathbf{S}_{i+\hat{y}} \cdot \hat{y} + \mathbf{S}_i \times \mathbf{S}_{i+\hat{z}} \cdot \hat{z}). \quad (1)$$

S_i is the unit vector in the direction of the magnetization at the site i of a three-dimensional cubic lattice and $< i, j >$ denote pairs of nearest-neighbor spins. The first term describes the ferromagnetic nearest-neighbor exchange with $J < 0$, the second term is the Zeeman interaction, and the third term stands for the Dzyaloshinskii-Moriya (DM) interaction. The DM constant $D = J \tan(2\pi/p)$ defines the period of modulated structures p. It was established by direct calculations that in chiral ferromagnets the DM interactions strongly suppress demagnetization effects[2,5]. In many practical cases the surface and internal stray-field magnetostatic energy of skyrmions can be reduced to local energy contributions and included into effective magnetic anisotropy energy[2,5].

In what follows, we use $J = 1$ and the DM constant is set to 0.445 which corresponds to $p = 15$. We consider periodic boundary conditions in z and x directions, whereas along y the stripe is confined by vertical surfaces with the free boundary conditions (Fig. 1). The size of our numerical grid is set to $2p \times 50 \times p$. In an infinite sample, below the critical field $H_D = D^2/2J$, the global minimum of (1) corresponds to the modulation phase with the propagation direction along the applied field, the *cone* phase[19] (Fig. 1 (c)):

$$\theta_c = \arccos(H/H_D), \qquad \psi_c = 2\pi z/p, \quad (2)$$

where θ, ψ are the polar and azimuthal angles of the magnetization vector.

The saturated state with $\theta = 0$ occurs when $H > H_D$. In the saturated state, isolated skyrmions are axisymmetric and translationally invariant along z[1,2]. Chiral surface twists for $H > H_D$ have been investigated in a number of earlier contributions[14–16]. Below H_D, the incompatibility with the longitudially modulated conical phase imposes a complex, three-dimensional character on the magnetic modulations of the skyrmions and edge states (Figs. 2-3).

The solutions for edge states in the sample with the conical phase (2) in its bulk are shown in Fig. 2. The dependence $S_z(y)$ for a fixed value of x and z (Fig. 2 (a)) shows the formation of two humps in the vicinity of two free surfaces xz with $y = 0$ and $y = L_y$. The S_z-component in these humps is larger than that for the cone in the middle of the sample and for some cross-sections ($z = 5, 12$) it even goes through the state co-aligned with the field, $S_z = 1$ (shaded regions in Fig. 2 (a) and the color plots in Fig. 2 (b)). As the edge states are incompatible with the conical phase, they are surrounded by a strip-like "shell" - a transitional region running parallel to the boundary. The shell has the higher energy density as compared with the conical phase (Fig. 2 (c)) and positive exponentially decaying asymptotics.

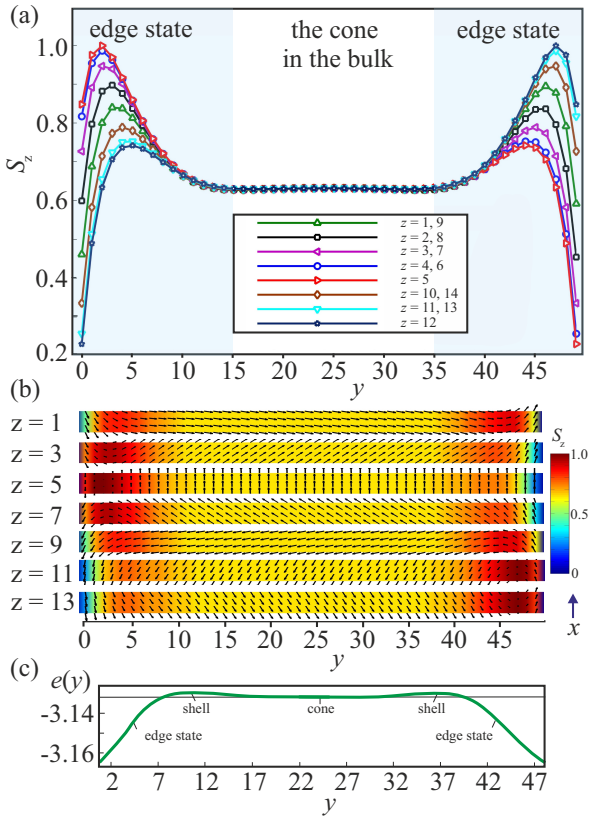

FIG. 2. (color online) Edge states in a film of a chiral magnet with the conical phase (2). (a) Variations of the magnetization component S_z along the y coordinate for fixed values of z. The blue shading indicates the regions occupied by the edge states. (b) color plots of $S_z(x; y)$ in a xy plane with fixed values of ψ_c and z. The black arrows show in-plane spin-components. (c) The energy density $e(y)$ averaged over z (green solid line). The black thin line shows the energy density in the conical phase. The energy density is divided into constituent parts: the energy distribution near the edges, in the conical phase and in the shell which is formed due to the incompatibility of the spin structures at the edges and the conical phase in the middle of the sample.

Fig. 3 shows color plots of the energy density $w(x; y; z = \text{const})$ and skyrmion energy densities averaged over the z-coordinate, $e(\rho) = (1/p) \int_0^p w dz$, and plotted along the radial directions for isolated skyrmions within the conical phase ($H/H_D = 0.6$, Fig. 3 (a)) and

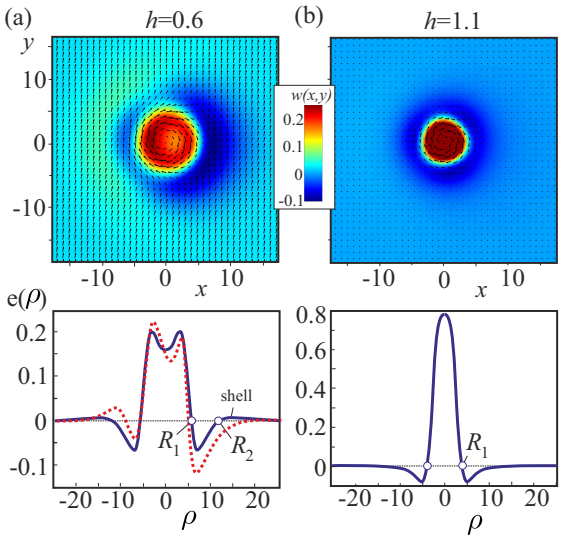

FIG. 3. (color online) Numerical solutions for isolated skyrmions obtained within the continuum version of the model (1). In (a) and (b) the isolated skyrmions are placed within different backgrounds - within the conical phase for $H/H_D = 0.6$ and the saturated state for $H/H_D = 1.1$, respectively. The first horizontal row shows two color plots of the energy density distributions $w(x; y; z = \text{const})$. The energy density is measured in units A/D^2 where A and D are the constants of the exchange ($A\,(\mathbf{grad}\,\mathbf{m})^2$) and DM ($D\,\mathbf{m}\cdot\mathrm{rot}\,\mathbf{m}$) interactions in the continuum version of (1). In the second row the energy density $e(\rho)$ is averaged over the z-coordinate and plotted across the skyrmionic centers. The red dotted line shows the cross-section of the color plot $w(x; y; z = \text{const})$. The characteristic radius R_2 signifies the formation of a skyrmionic shell with positive energy over the conical phase (see also Supplementary Movie).

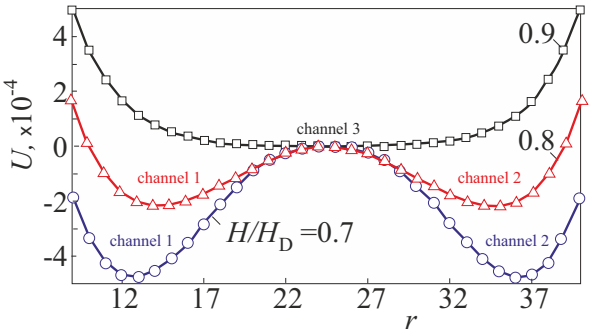

FIG. 4. (color online). The skyrmion-edge potential energy U vs. the distance r between the skyrmion center and the edge of the sample. The potential energy is measured with respect to the energy of a system for $r = L_y/2$, which corresponds to a skyrmion in the middle of the sample. $U(r)$ was calculated by imposing the constraint, $S_z = -1$, at the skyrmion center and minimizing the energy with respect to spins at all other sites. The local minima of $U(r)$ give rise to a sequence of edge channels: channels numbered 1 and 2 are located at the boundaries of the sample for $H < H_D$, and the channel 3 runs along the sample center for $H > H_D$. These channels, separated by the potential barriers, guide the motion of skyrmions.

within the saturated state ($H/H_D = 1.1$, Fig. 3 (b)). For $H > H_D$, a characteristic radius R_1 specifies the size of the skyrmionic core. The core ($\rho < R_1$) with the positive energy density is surrounded by the ring ($\rho > R_1$) with the negative energy density which is known to form due to the DM interaction and protects isolated skyrmions from collapse[1]. The ring has the radial symmetry in all layers with the fixed z-coordinate (the color plot of $w(x; y; z = \text{const})$ in Fig. 3 (b)). For $H < H_D$, $e(\rho)$ has two characteristic radii R_1 and R_2. The skyrmionic shell is the part of the non-axisymmetric skyrmion with $\rho > R_2$ and represents an outer ring[18] with the positive energy density. The color plot in Fig. 3 (a) also shows that the ring with the negative energy density is partially weakened. This occurs along the radial directions where the magnetization rotates from the state opposite to the field in the center (polar angle of the magnetization $\theta = \pi$) directly to θ_c. On the contrary, the ring is restored in those parts where the magnetization rotation goes to θ_c via the state with $\theta = 0$. The attraction between skyrmions and the edges of the track occurs because the total energy can be reduced if their respective shells overlap. The skyrmion-edge interaction potentials as a function of a distance r between the skyrmion center and the ($y = 0$)-edge of the sample for different values of the applied magnetic field are plotted in Fig. 4. Potential profiles show that the attractive skyrmion-edge coupling is characterized by a rather deep potential well establishing the equilibrium separation of skyrmions from the edges. The distance $r_{min} = \min(r)$ increases rapidly with the field. And already for $H/H_D = 0.9$ skyrmions are "released" by the edge states and are pushed to the center of the sample.

Our results open completely new perspectives on using skyrmions in nanoelectronic devices with the conical phase. First of all, the edge states with the complex spin structure give rise to a formation of two edge "channels" (schematically shown by red strips in Fig. 1) which run along boundaries of chiral magnets and guide the skyrmions. These channels correspond to the minima of skyrmion-edge interaction potentials (Fig. 4). The distance of channels from boundaries effectively depends on the value of the applied magnetic field: for $H/H_D = 0.8$ (red line with triangular markers in Fig. 4) the channels are located farther from the boundaries and closer to each other than for $H/H_D = 0.7$ (blue line with circular markers in Fig. 4). For some threshold field H_{tr}, two channels numbered 1 and 2 in Figs. 1 and 4 merge into one channel 3 along the middle of the sample. The threshold field of this phenomenon depends mainly on the confinement ratio ν – the ratio of p to the width of the racetrack L_y. Due to the field-dependent position of channels, channels 1 and 2 may overlap and form the channel 3 for the fields lower than H_D in narrow films. In particular, the sample used in the numerical simulations ($\nu = L_y/p = 49/15 = 3.27$) exhibits one central

channel already for $H/H_D = 0.9$ in spite of the stable conical phase. H_{tr} gradually increases for wider films and reaches H_D for infinitely wide samples.

We also note that for samples confined by parallel surfaces along z-axis with $z = 0; L_z$, chiral surface twists additionally modify the structure of skyrmions near the surfaces[20]. These surface twists distort the translational invariance of skyrmions even in the saturated state and become evident in an additional twist of the azimuthal angle of the magnetization in skyrmions. We argue, however, that this fact does not change the attractive nature of the skyrmion-edge potential and subsequent effects.

The channel management by the applied magnetic field opens new ways to do logical operations with skyrmions on racetracks, as the information can be encoded in the lateral positions of skyrmions. Skyrmions, which fit perfectly into the edge channels, can be directed by currents along two lateral boundaries of a film and may be switched between channels by current pulses. As the potential barrier between two lateral channels is lower for larger values of the field, the lower current densities are needed to switch skyrmions between two channels. On the contrary, to ensure that the skyrmions do not jump from one channel to another due to the skyrmion Hall effect, the magnetic field must be decreased leading to the higher potential barrier between channels. Moreover, the consecutive order of skyrmions is also influenced by the value of the field, as isolated skyrmions within the conical phase attract each other and form clusters with the field-dependent inter-skyrmion distance (see for details Ref. 18). This may help to avoid clogging of skyrmionic bits as encountered in Ref. 17.

To summarize, our data have clearly demonstrated that the skyrmion-edge attraction develops in the presence of the longitudinally modulated phases and may play an important role in skyrmion-based spintronic devices (e.g. a racetrack memory design). In particular, it can be employed for magnetic patterning of nanodevices. The mechanism of skyrmion-edge attraction stems from the complex spin structures of the edge states formed at the boundaries of confined helimagnets for $H < H_D$ and isolated skyrmions embraced by the conical phase. Our results are relevant not only to the application of magnetic skyrmions in memory technology, but also elucidate the fundamental properties of skyrmions and the edge states formed in the conical phases of chiral magnets.

The authors are grateful to M. Mostovoy and T. Monchesky for useful discussions. A.O.L acknowledges financial support by the FOM grant 11PR2928. A.N.B acknowledges support by the Deutsche Forschungsgemeinschaft via Grant No. BO 4160/1-1.

* A.Leonov@ifw-dresden.de

[1] A. O. Leonov, T. L. Monchesky, N. Romming, A. Kubetzka, A. N. Bogdanov, R. Wiesendanger, New J. of Phys. **18**, 065003 (2016).

[2] A. Bogdanov and A. Hubert, J. Magn. Magn. Mater. **138**, 255 (1994).

[3] N. Romming, C. Hanneken, M. Menzel, J. E. Bickel, B. Wolter, K. von Bergmann, A. Kubetzka, R. Wiesendanger, Science **341**, 636 (2013); N. Romming, A. Kubetzka, C. Hanneken, K. von Bergmann, R. Wiesendanger, Phys. Rev. Lett. **114**, 177203 (2015).

[4] J. Iwasaki, M. Mochizuki, N. Nagaosa, Nat. Nanotechnol. **8**, 742 (2013).

[5] N. S. Kiselev, A. N. Bogdanov, R. Schaefer, U. K. Roessler, J. Phys. D: Appl. Phys. **44**, 392001 (2011).

[6] A. Fert, V. Cros, J. Sampaio, Nat. Nanotechnol. **8**, 152 (2013).

[7] E. M. R. Tomasello, R. Zivieri, L. Torres, M. Carpentieri, and G. Finocchio, Sci. Rep. **4**, 6784 (2014).

[8] C. Moreau-Luchaire, , C. Moutafis, N. Reyren, J. Sampaio, C. A. F. Vaz, N. Van Horne, K. Bouzehouane, K. Garcia, C. Deranlot, P. Warnicke, P. Wohlhüter, J.-M. George, M. Weigand, J. Raabe, V. Cros, A. Fert, Nat. Nanotechnol. **11**, 444 (2016).

[9] S. Woo, K. Litzius, B. Kruger, M. Y. Im, L. Caretta, K. Richter, M. Mann, A. Krone, R. M. Reeve, M. Weigand, P. Agraval, I. Lemesh, M. A. Miawass, P. Fisher, M. Klaui, G. R. S. D. Beach, Nat. Mater. **15**, 501 (2016).

[10] X. Z. Yu, N. Kanazawa, W. Z. Zhang, T. Nagai, T. Hara, K. Kimoto, Y. Matsui, Y. Onose, Y. Tokura, Nat. Commun. **3**, 988 (2012).

[11] C. Hanneken, A. Kubetzka, K. von Bergmann, R. Wiesendanger, New J. Phys. **18**, 055009 (2016).

[12] H. F. Du, R. C. Che, L. Y. Kong, X. B. Zhao, C. M. Jin, C. Wang, J. Y. Yang, W. Ning, R. W. Li, C. Q. Jin, X. H. Chen, J. D. Zang, Y. H. Zhang, M. L. Tian, Nat. Commun. **6**, 8504 (2015); H. F. Du, J. P. DeGrave, F. Xue, D. Liang, W. Ning, J. Y. Yang, M. L. Tian, Y. H. Zhang, S. Jin, Nano Lett., **14**, 2026 (2014).

[13] For an overview of this phenomenon and bibliogrphy see[14].

[14] S. A. Meynell, M. N. Wilson, H. Fritzsche, A. N. Bogdanov, T. L. and Monchesky, Phys. Rev. B **90**, 014406 (2014).

[15] M. N. Wilson, E. A. Karhu, D. P. Lake, A. S. Quigley, S. Meynell, A. N. Bogdanov, H. Fritzsche, U. K. Rößler, and T. L. Monchesky, Phys. Rev. B **88**, 214420 (2013).

[16] R. Keesman, A. O. Leonov, S. Buhrandt, G. T. Barkema, L. Fritz, R. A. Duine, Phys. Rev. B **92**, 134405 (2015).

[17] X. C. Zhang, G. P. Zhao, H, Fangohr, J. P. Liu, W. X. Xia, J. Xia, F. J. Morvan, Sci. Rep. **5**, 7643 (2015).

[18] A. O. Leonov, T. L. Monchesky, J. C. Loudon, A N Bogdanov, J. Phys.: Condens. Matter. **28**, 35LT01 (2016).

[19] P. Bak P and M. H. Jensen, J. Phys.C: Solid State Phys. **13**, L881 (1980).

[20] A. O. Leonov, Y. Togawa, T. L. Monchesky, A. N. Bogdanov, J. Kishine, Y. Kousaka, M. Miyagawa, T. Koyama, J. Akimitsu, Ts. Koyama, K. Harada, S. Mori, D. McGrouther, R. Lamb, M. Krajnak, S. McVitie, R. L. Stamps, K. Inoue, Phys. Rev. Lett. **117**, 087202 (2016).